Electronic Supplementary Material (ESI) for Dalton Transactions.
This journal is © The Royal Society of Chemistry 2021

Supporting Information

Metal-radical hetero-tri-spin SCM with methyl-pyrazole-nitronyl nitroxide bridges

Xiaohui Huang,[1] Kang Wang,[1] Jing Han,[1] Junfang Xie,[1] Licun Li*[1] and Jean-Pascal Sutter*[2]

[1] *Department of Chemistry, Key Laboratory of Advanced Energy Materials Chemistry, College of Chemistry, Nankai University, Tianjin 300071, China*

[2] *Laboratoire de Chimie de Coordination du CNRS (LCC-CNRS), Université de Toulouse, CNRS, Toulouse, France*

* *Corresponding author. E-mail address:*

llicun@nankai.edu.cn

sutter@lcc-toulouse.fr

Contents

Table S1. Selected bond lengths [Å] and bond angles [°] for **1** 3

Table S2. Selected bond lengths [Å] and bond angles [°] for **2** 3

Table S3. Selected bond lengths [Å] and bond angles [°] for **3** 3

Table S4. SHAPE analysis for the Ln coordination spheres for **1–3**.....4

Figure S1. The coordination polyhedron of Gd^{III} ion in **1**.....4

Figure S2. The chain structure of complex **2.** 5

Figure S3. The coordination polyhedron of Tb^{III} ion in **2.** 5

Figure S4. The chain structure of complex **3.** 5

Figure S5. The coordination polyhedron of Dy^{III} ion in **3**.....6

Figure S6. Packing diagram of **1.** 6

Figure S7. Packing diagram of **2** 7

Figure S8. Packing diagram of **3.** 7

Figure S9. Powder X-ray diffraction patterns of complex **1-3.** 8

Figure S10. Plot of $\chi_M T$ versus T for **3**.....8

Figure S11. *M* versus *H* plot for **2** and **3** at 2 K.....9

Figure S12. Plot of ln($\chi_M'T$) versus *1/T* recorded in zero-field for (left) **2** and (right) **3**; the solid red line is the best fit of the Glauber's expression to the linear part 8-23 K for **2** and 5-15 K for **3**.....9

Figure S13. (left) Temperature of the AC susceptibility for **2** in the frequency range 1-1488 Hz in zero field for compound **2**; (right) detail of the χ_M'' versus *T* behavior..10

Figure S14. Selection of deconvolution of χ_M'' versus *T* (H_{DC} = 0) for **2** for different frequencies. The dashed line is the fit of two Gaussian functions; C1 and C2 have been plotted with the best-fit parameters 11

Figure S15. Temperature and Frequency dependence of χ_M'' for **2** in H_{DC} = 1 kOe. .11

Figure S16. Experimental χ_M' and χ_M'' versus frequency for **2** (in zero field) with best fit (full red lines, for data from 2.0 to 2.8 K) of an expression of two Debye models to account for the two relaxation processes.....11

Figure S17. lnτ versus 1/T plots for compound **2** and best fit (solid lines) of the Arrhenius law. The τ values have been derived from the *T* of the maximum of C1 and C2 components deconvoluted from experimental χ_M'' versus *T* behaviors.....12

Figure S18. Cole-Cole plots with best fits (full lines). The distribution widths of the relaxation times, α , are large, ranging from 0.12 to 0.33 for C1 and 0.41 to 0.51 for the SCM (C2), likely resulting from the merging of the two data sets.....12

Figure S19. Temperature-dependent ac signals of the χ_M' and χ_M'' for compound **3** in (left) zero field and (right) H_{DC} = 1 kOe field.....13

Table S1. Selected bond distances (Å) and angles (°) for compound **1**.

1 Gd			
Gd(1)-O(2)	2.359(7)	Gd(1)-O(3)	2.322(7)
Gd(2)-O(6)	2.372(7)	Gd(2)-O(7)	2.299(7)
N(3)-O(2)	1.304(10)	N(5)-O(3)	1.294(10)
Cu(1)-N(1)	2.340(9)	Cu(1)-N(16)	2.489
Cu(2)-N(10)	2.396(11)	Cu(2)-N(7)	2.320(9)
N(3)-O(2)-Gd(1)	134.0(6)	N(5)-O(3)-Gd(1)	148.6(6)
N(12)-O(6)-Gd(2)	134.0(7)	N(14)-O(7)-Gd(2)	164.0(6)
O(13)-Gd(1)-O(14)	71.8(3)	O(16)-Gd(1)-O(15)	72.5(2)
O(17)-Gd(1)-O(18)	71.4(2)	O(24)-Gd(2)-O(23)	72.6(3)
O(25)-Gd(2)-O(26)	72.9(3)	O(27)-Gd(2)-O(28)	71.6(3)
O(10)-Cu(1)-O(9)	91.8(3)	O(12)-Cu(1)-O(11)	92.6(3)
O(20)-Cu(2)-O(19)	92.8(4)	O(22)-Cu(2)-O(21)	91.9(3)
Gd(1)-O(2)-N(3)-C(5)	90.93(1)	Gd(1)-O(2)-N(5)-C(18)	-110.20(1)
Gd(2)-O(6)-N(12)-C(27)	95.62(1)	Gd(2)-O(7)-N(14)-C(40)	168.08(2)

Table S2. Selected bond distances (Å) and angles (°) for compound **2**.

2 Tb			
Tb(1)-O(2)	2.301(4)	Tb(1)-O(3)	2.345(4)
Tb(2)-O(6)	2.288(5)	Tb(2)-O(7)	2.356(5)
Cu(1)-N(1)	2.293(5)	Cu(1)-N(16)	2.408(6)
Cu(2)-N(10)	2.488(5)	Cu(2)-N(7)	2.334(5)
N(3)-O(2)-Tb(1)	147.8(4)	N(5)-O(3)-Tb(1)	133.4(3)
N(12)-O(6)-Tb(2)	165.8(4)	N(14)-O(7)-Tb(2)	135.5(5)
O(14)-Tb(1)-O(13)	72.05(15)	O(15)-Tb(1)-O(16)	72.62(15)
O(18)-Tb(1)-O(17)	72.35(15)	O(23)-Tb(2)-O(24)	72.47(18)
O(25)-Tb(2)-O(26)	71.91(17)	O(27)-Tb(2)-O(28)	73.60(18)
O(10)-Cu(1)-O(9)	91.9(2)	O(11)-Cu(1)-O(12)	91.74(19)
O(20)-Cu(2)-O(19)	91.50(18)	O(22)-Cu(2)-O(21)	92.70(17)

Table S3. Selected bond distances (Å) and angles (°) for compound **3**.

3 Dy			
Dy(1)-O(2)	2.341(5)	Dy(1)-O(3)	2.297(6)
Dy(2)-O(6)	2.359(6)	Dy(2)-O(7)	2.285(5)
Cu(1)-N(1)	2.343(6)	Cu(1)-N(16)	2.496(6)
Cu(2)-N(10)	2.412(8)	Cu(2)-N(7)	2.315(7)
N(3)-O(2)-Dy(1)	132.5(4)	N(5)-O(3)-Dy(1)	148.3(5)
N(12)-O(6)-Dy(2)	135.5(6)	N(14)-O(7)-Dy(2)	165.0(5)
O(13)-Dy(1)-O(14)	72.37(19)	O(16)-Dy(1)-O(15)	73.3(2)
O(18)-Dy(1)-O(17)	71.90(19)	O(24)-Dy(2)-O(23)	72.5(2)
O(25)-Dy(2)-O(26)	74.7(2)	O(27)-Dy(2)-O(28)	72.0(2)
O(10)-Cu(1)-O(9)	91.5(2)	O(11)-Cu(1)-O(12)	93.1(2)
O(20)-Cu(2)-O(19)	91.7(3)	O(21)-Cu(2)-O(22)	91.6(2)

Table S4. SHAPE analysis for the Ln coordination spheres for **1**-**3**.

Compound	SAPR-8	**TDD-8**	JBTPR-8	BTPR-8	JSD-8
Gd1	2.207	**0.362**	2.174	1.685	2.527
Gd2	1.879	**0.606**	1.891	1.464	2.998
Tb1	2.268	**0.354**	2.163	1.721	2.459
Tb2	1.800	**0.527**	1.953	1.524	3.030
Dy1	2.340	**0.343**	2.196	1.754	2.459
Dy2	1.887	**0.540**	1.998	1.598	3.019

SAPR-8: Square antiprism; TDD-8: Triangular dodecahedron; JBTPR-8: Biaugmented trigonal prism J50; BTPR-8: Biaugmented trigonal prism; JSD-8: Snub diphenoid J84.

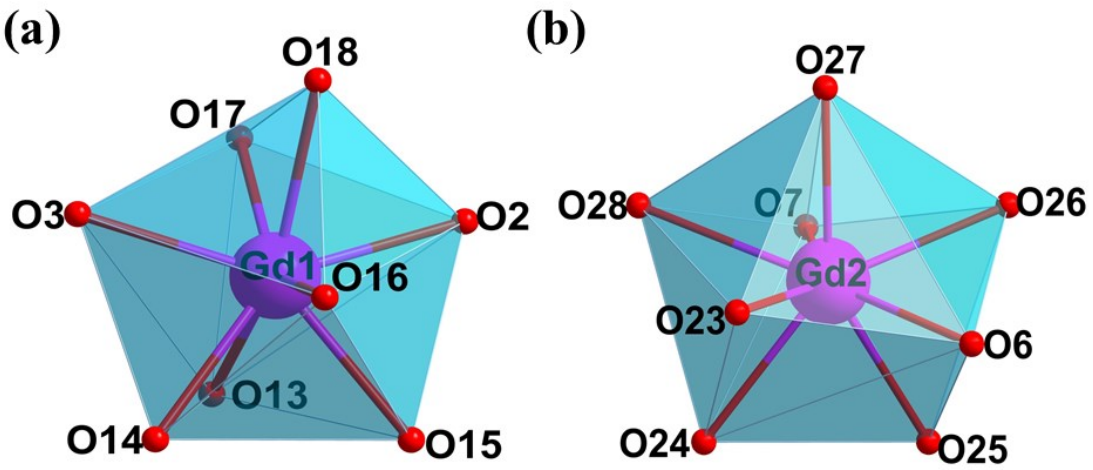

Fig. S1 The coordination polyhedron of Gd^{III} ion in complex **1** (left) Gd1; (right) Gd2.

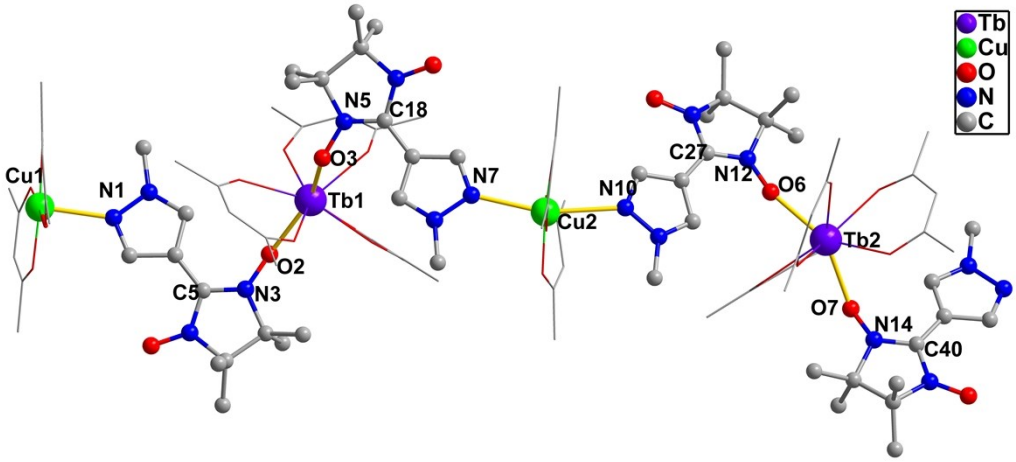

Fig. S2 The chain structure of complex **2**. H and F atoms are not shown for the sake of clarity.

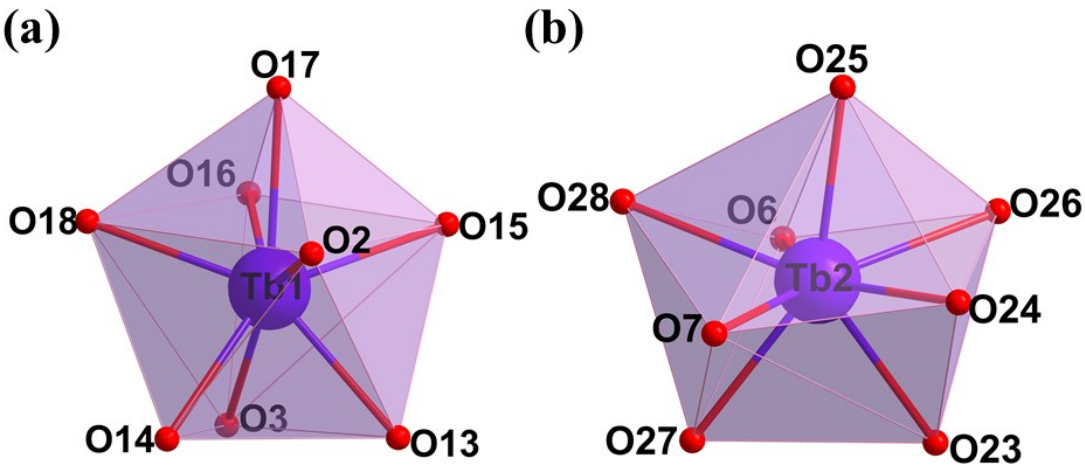

Fig. S3 The coordination polyhedron of Tb^{III} ion in complex **2**. (left) Tb1; (right) Tb2.

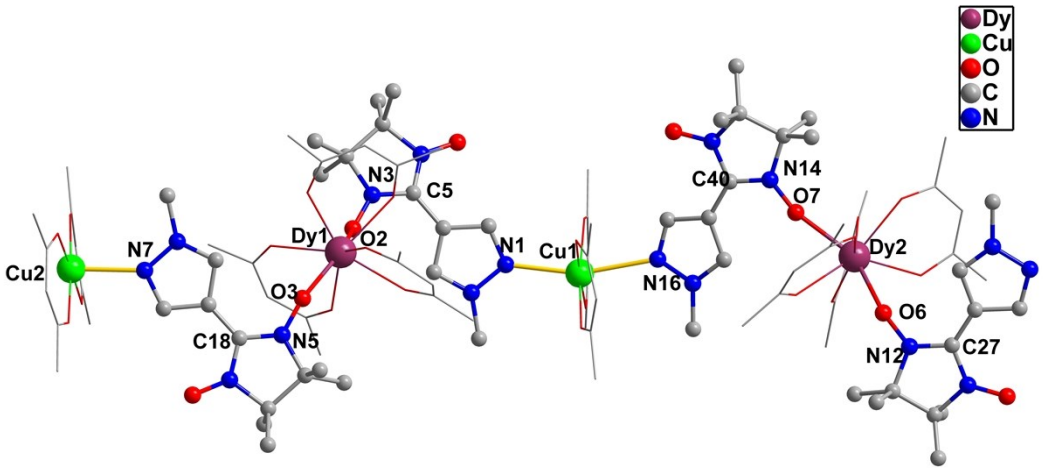

Fig. S4 The chain structure of complex **3**. H and F atoms are not shown for the sake of clarity.

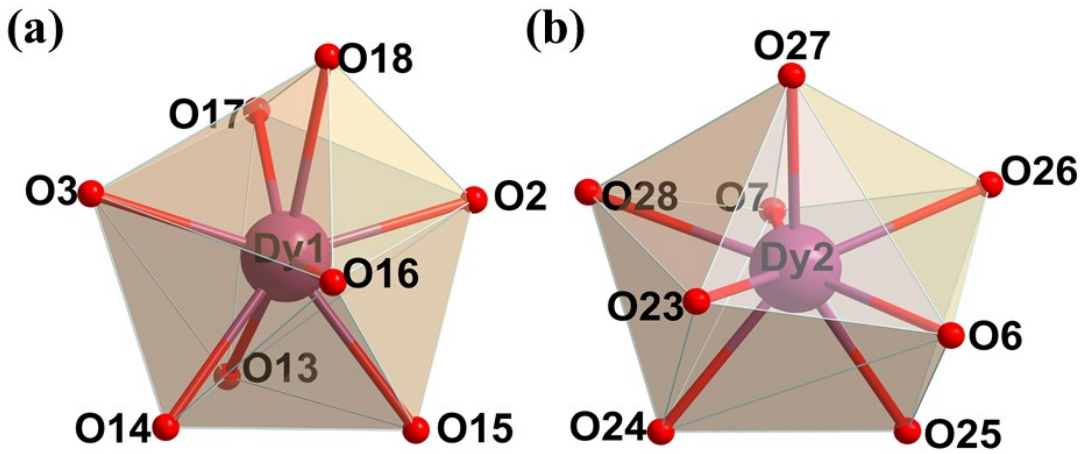

Fig. S5 The coordination polyhedron of Dy^{III} ion in complex **3**. (left) Dy1; (right) Dy2.

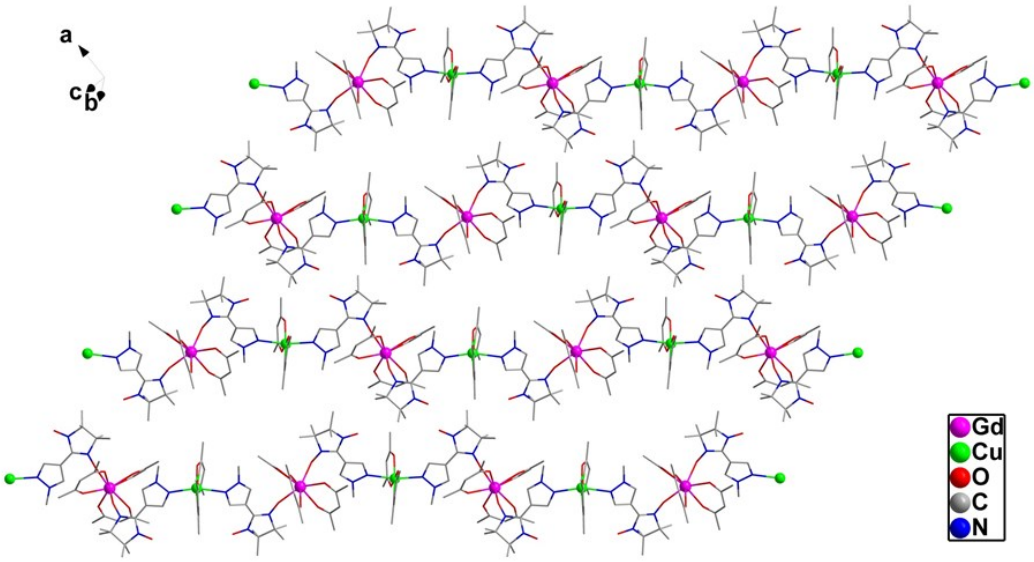

Fig. S6 Packing diagram of **1** (H and F atoms are omitted for clarity).

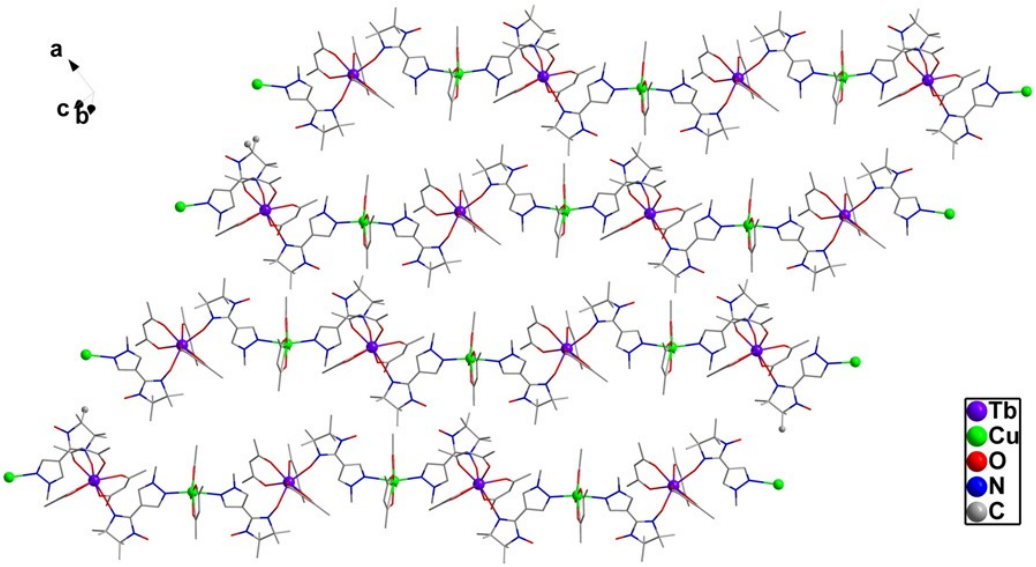

Fig. S7 Packing diagram of **2** (H and F atoms are omitted for clarity).

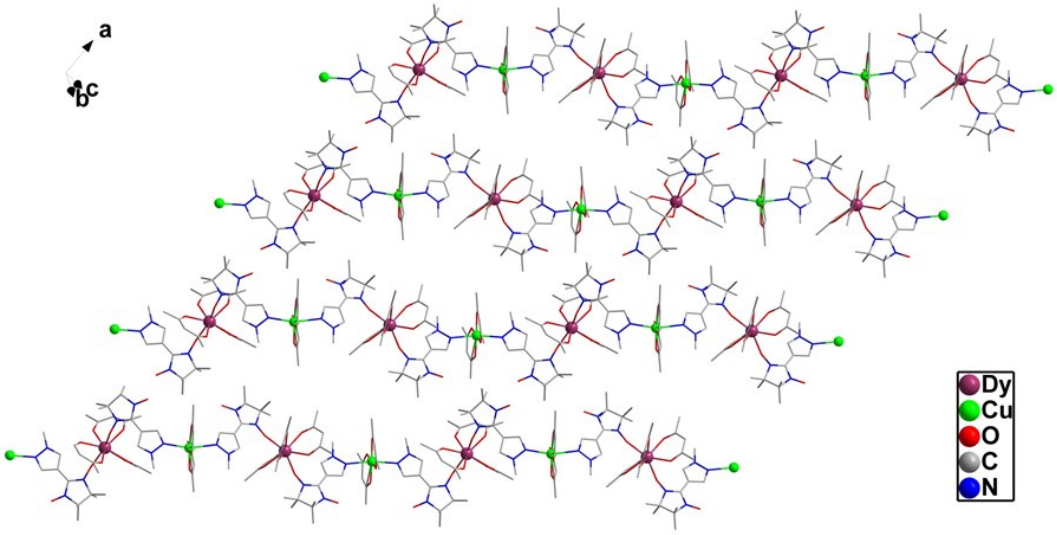

Fig. S8 Packing diagram of **3** (H and F atoms are omitted for clarity).

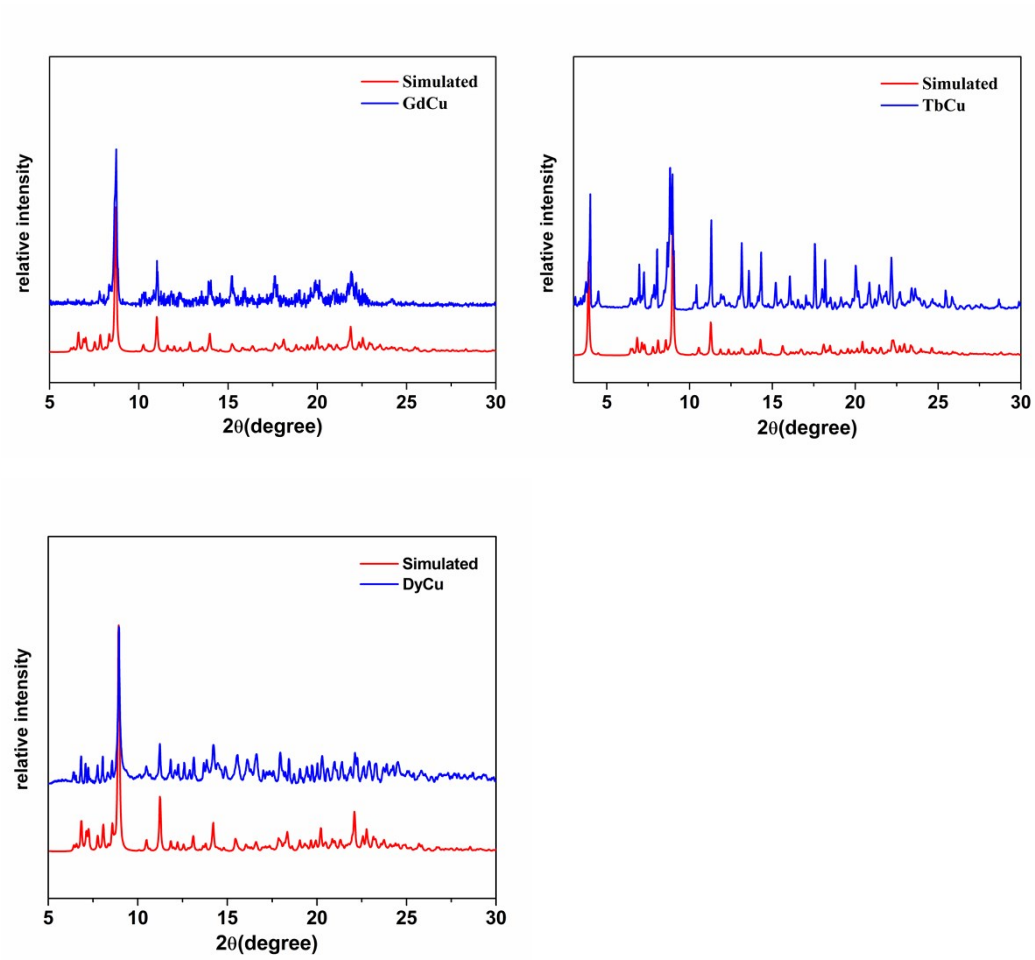

Fig. S9 Powder X-ray diffraction patterns of complexes **1**-**3** at room temperature.

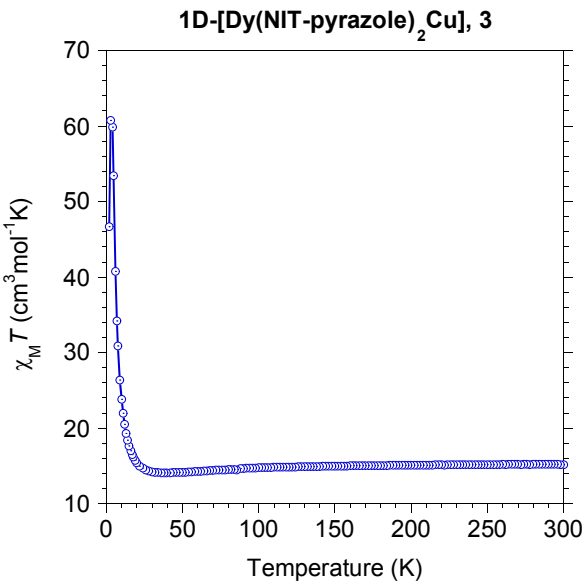

Fig. S10 Plot of $\chi_M T$ versus T for **3**.

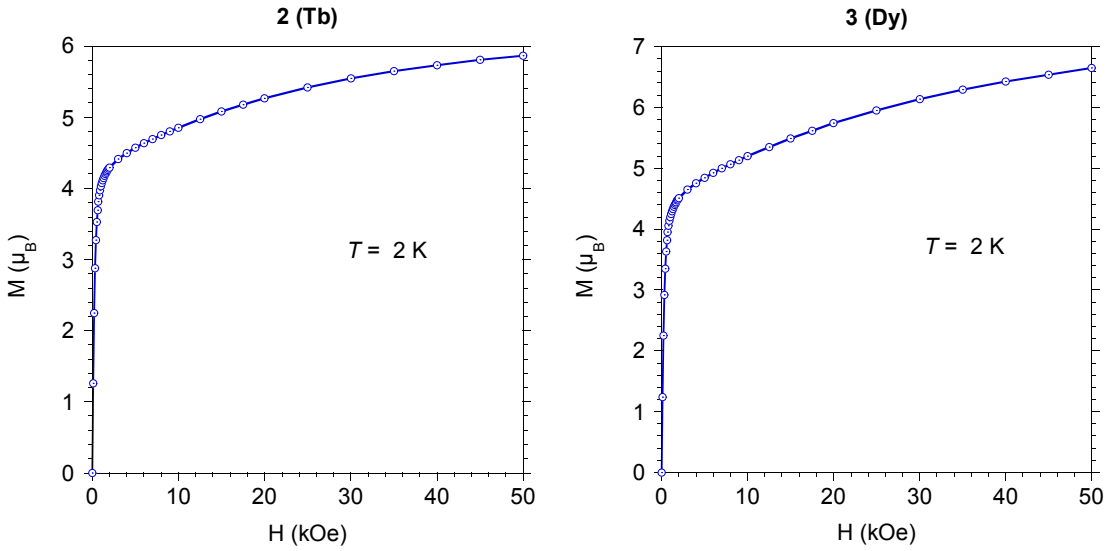

Fig. S11 Field-dependent magnetization for (left) **2** and (right) **3** at 2 K.

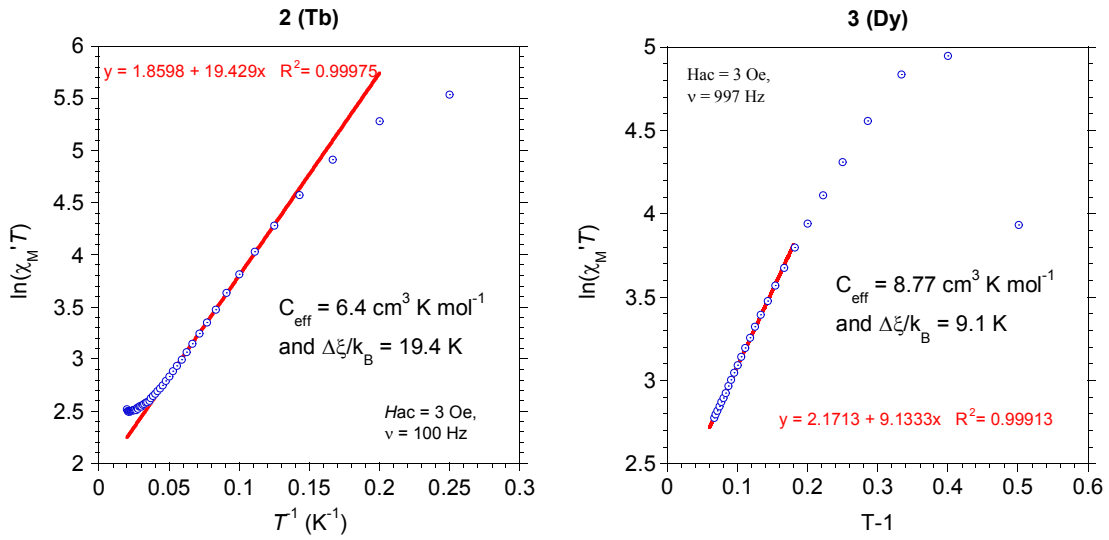

Fig. S12 Plot of ln($\chi_M'T$) versus *1/T* recorded in zero-field for (left) **2** and (right) **3;** the solid red line is the best fit of the Glauber's expression to the linear part 8-23 K for **2** and 5-15 K for **3**.

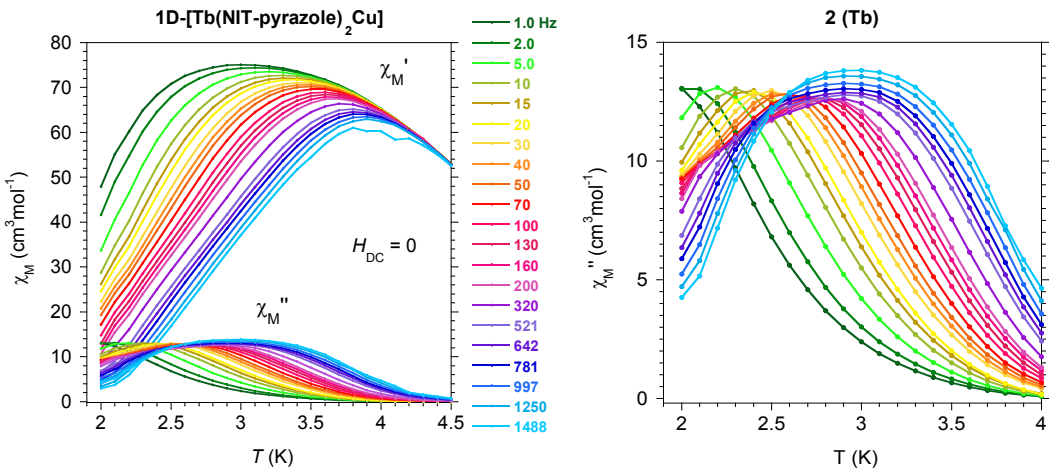

Fig. S13 *(left)* Temperature of the AC susceptibility for **2** in the frequency range 1-1488 Hz in zero field for compound **2**; *(right)* detail of the χ_M'' versus T behavior.

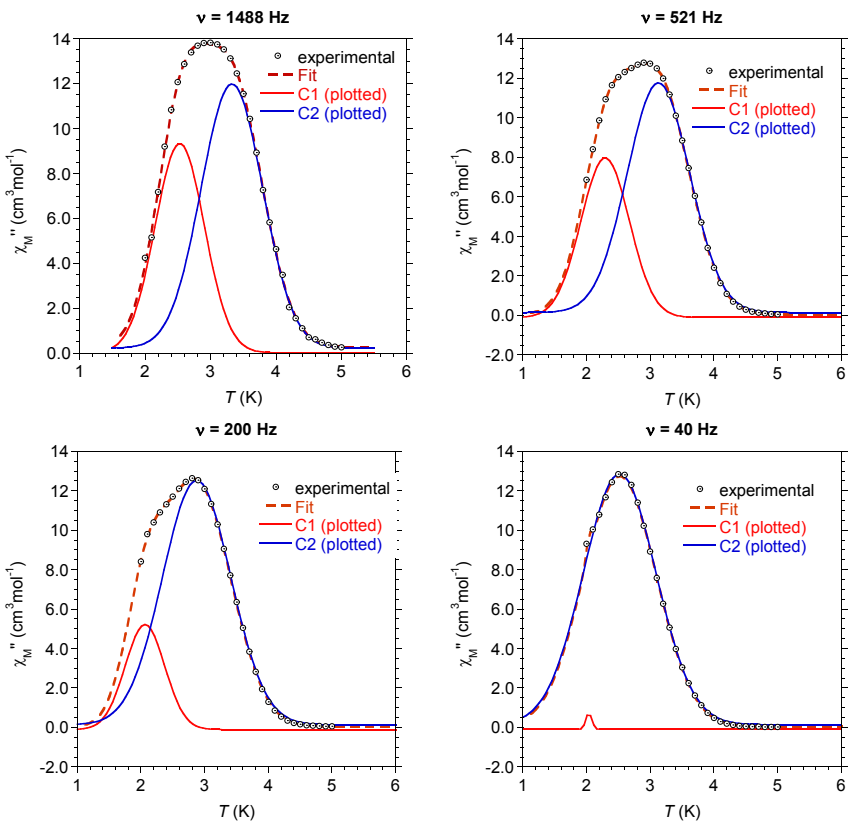

Fig. S14 Selection of deconvolution of χ_M'' versus T ($H_{DC} = 0$) for **2** for different frequencies. The dashed line is the fit of two Gaussian functions; C1 and C2 have been plotted with the best-fit parameters.

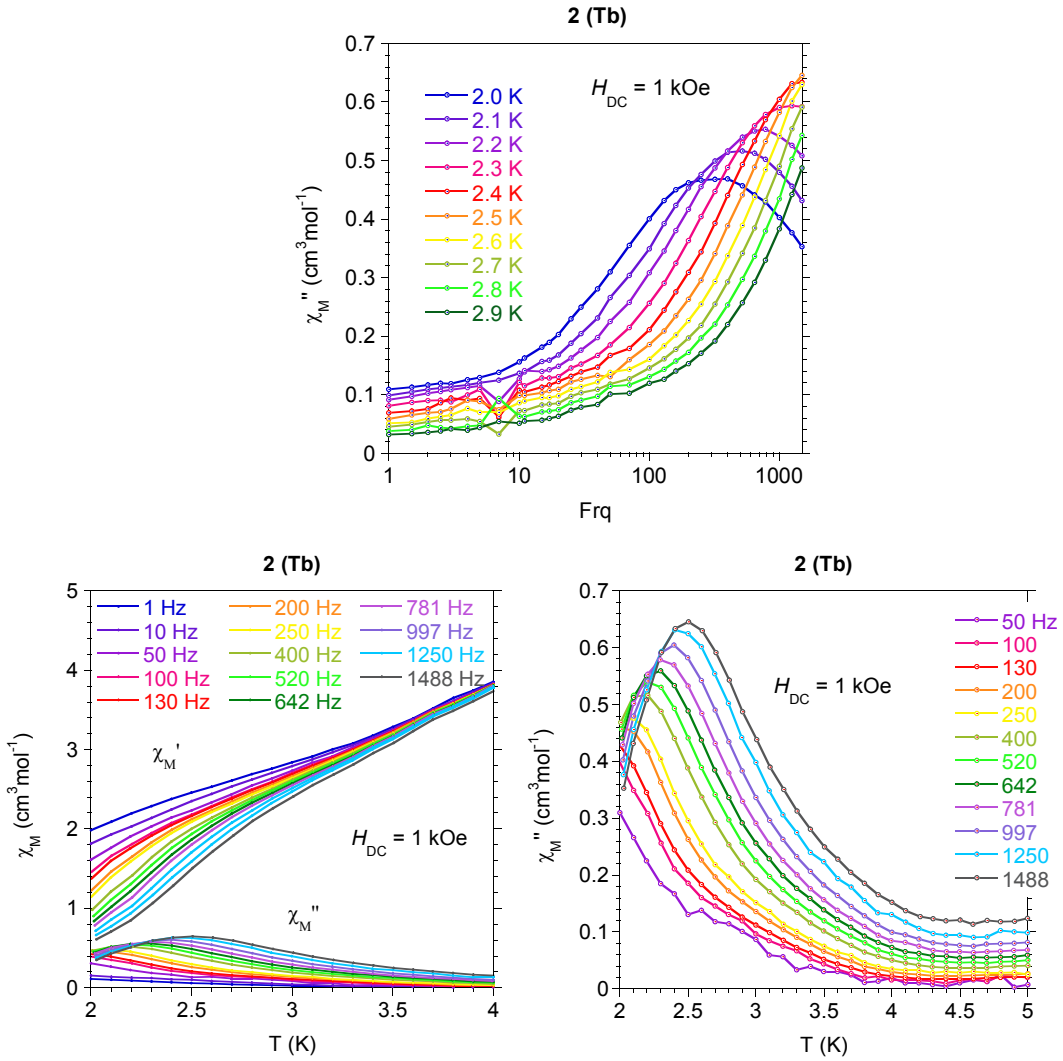

Fig. S15 Temperature and frequency dependence of χ_M' and χ_M'' for **2** in H_{DC} = 1 kOe

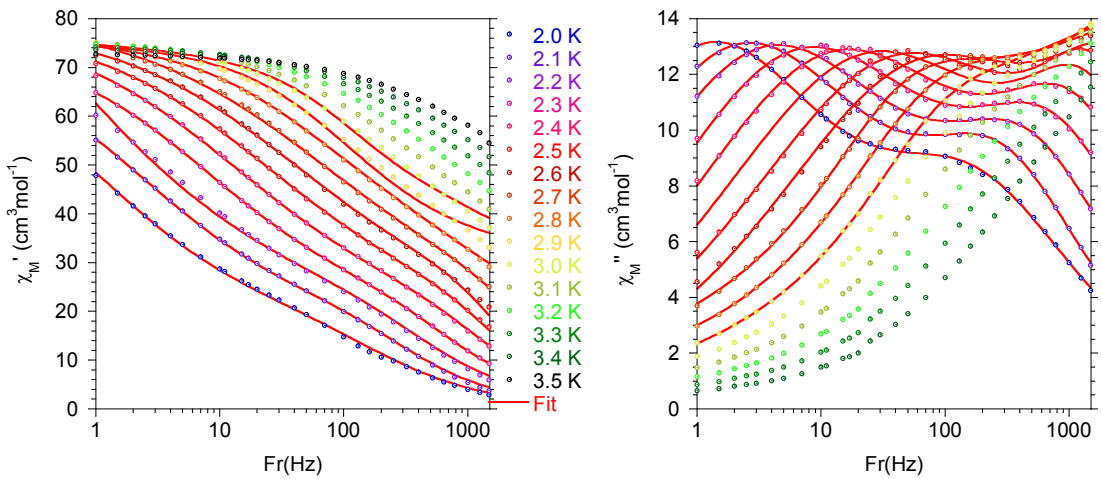

Fig. S16 Experimental χ_M' and χ_M'' versus frequency for **2** (in zero field) with best fit (full red lines, for data from 2.0 to 2.8 K) of an expression of two Debye models to account for the two relaxation processes. The resulting τ values are given in Figure 6c.

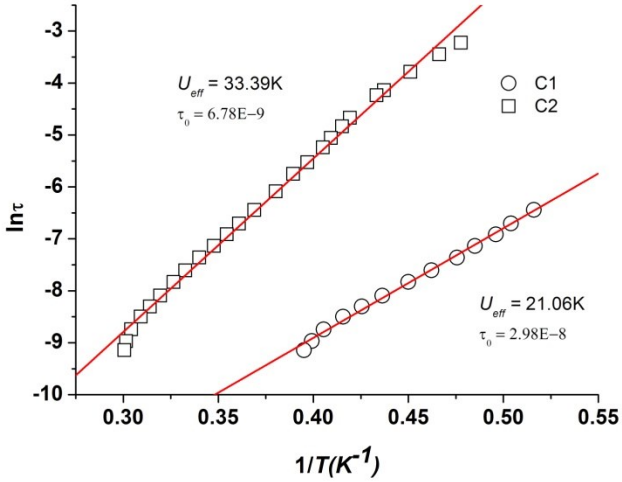

Fig. S17 lnτ versus 1/T plots for compound **2** and best fit (solid lines) of the Arrhenius law. The τ values have been derived from the *T* of the maximum of C1 and C2 components deconvoluted from experimental χ_M'' versus *T* behaviors.

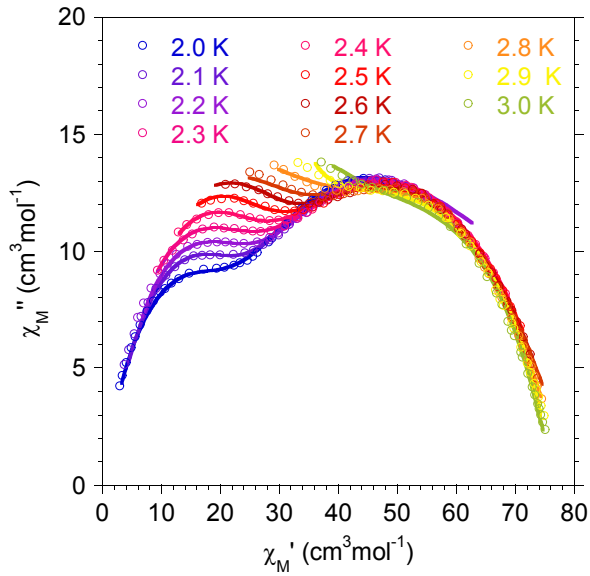

Fig. S18 Cole-Cole plots with best fits (full lines). The distribution widths of the relaxation times, α, are large, ranging from 0.12 to 0.33 for C1 and 0.41 to 0.51 for the SCM (C2), likely resulting from the merging of the two data sets.

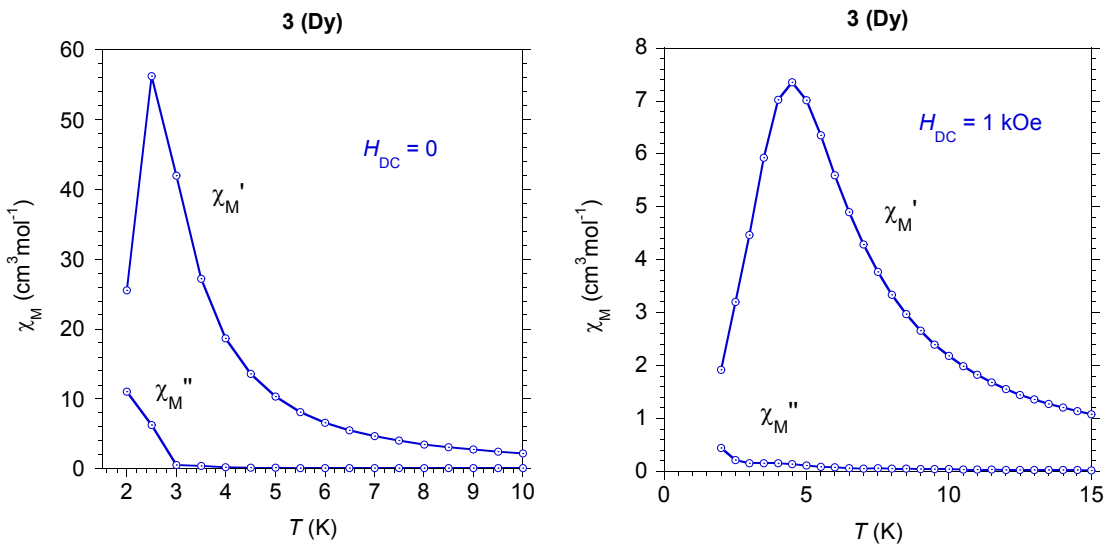

Fig. S19 Temperature-dependent ac signals of the χ_M' and χ_M'' for compound **3** in *(left)* zero field and *(right)* H_{DC} = 1 kOe field.